Journal of Materials Chemistry A

Accepted Manuscript

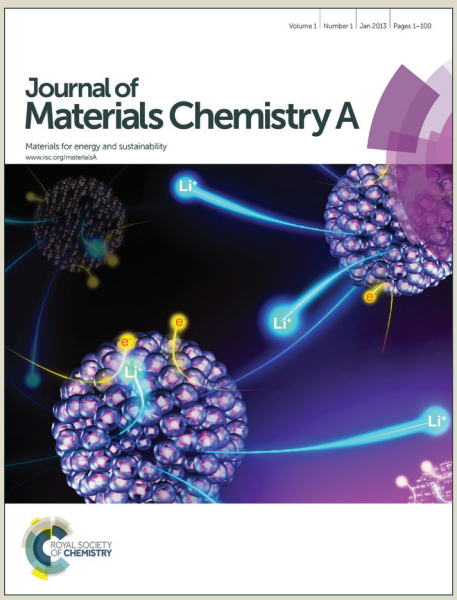

ROYAL SOCIETY OF CHEMISTRY

www.rsc.org/materialsA

Journal of Materials Chemistry A

Cite this: DOI: 10.1039/c0xx00000x

www.rsc.org/xxxxxx

ARTICLE TYPE

Ag/white graphene foam for catalytic oxidation of methanol with high efficiency and stability

Huijie Zhao,[1†] Jizhong Song,[1, 2†] Xiufeng Song,[2] Zhong Yan,[2] Haibo Zeng[2, 1]*

Received (in XXX, XXX) Xth XXXXXXXXX 200X, Accepted Xth XXXXXXXXX 200X
DOI: 10.1039/b000000x

Abstract: Oxidation of methanol not only eliminates the contamination of the typical volatile organic compounds (VOCs), but also provides clean energy. Here, we report Ag/white graphene foam to act as catalysts for the oxidation reaction of methanol with both high conversion efficiency and high stability. The T_{50} and T_{95} of Ag/white graphene foam catalysts are as low as 50 ^{o}C and 110 ^{o}C, almost the half of Ag/γ-Al_2O_3 catalysts. Furthermore, when the temperature was fixed at 100 ^{o}C, the 93% conversion efficiency of Ag/white graphene foam was well persisted with fluctuation less than 2% within 50 hours, while conversion efficiency of Ag/γ-Al_2O_3 degraded sharply from 46% to 30%. Such outstanding catalytic performance of Ag/white graphene foam is mainly attributed to the unique microstructure, especially the multi-level pores and few-layer atomically thin walls, which has been well confirmed by the SEM and TEM observations.

TOC Graphic

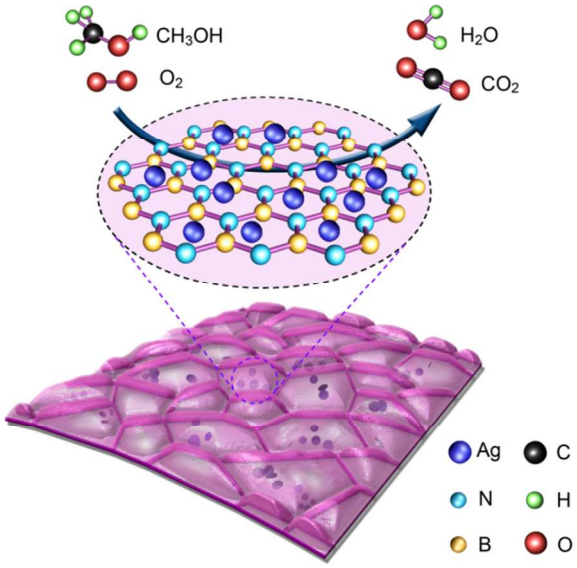

[1]State Key Laboratory of Mechanics and Control of Mechanical Structures & College of Materials Science and Technology, Nanjing University of Aeronautics and Astronautics, Nanjing 210016, China
[2]Institute of Optoelectronics & Nanomaterials, College of Materials Science and Engineering, Nanjing University of Science and Technology, Nanjing 210094, China
[†]These authors contributed equally to this work.
*Correspondence and requests for materials should be addressed to H.B.Z. (zeng.haibo@njust.edu.cn)

Journal of
Materials Chemistry A

Cite this: DOI: 10.1039/c0xx00000x

www.rsc.org/xxxxxx

ARTICLE TYPE

1 Introduction

Oxidation conversion of methanol has attracted great interest due to the demands of environment-friendly and energy-saving society. Methanol, an important organic chemical raw material and clean fuel, is colorless, transparent, and easily transported. Methanol as the typical representative of volatile organic compounds (VOCs), can be used for direct methanol fuel cells (DMFCs) and fueled vehicle (methanol gasoline, methanol diesel)[1-6]. However, it can cause serious environmental damage due to its toxicity and volatility. Therefore, reducing the pollution released by the VOCs (methanol) becomes a topic of great importance, which can be improved by increasing the catalytic efficiency of VOCs (methanol). [7-11]

The conversion efficiency is mainly associated with the key catalyst, co-catalyst, catalyst support and the third-group compounds[12]. As for a specific key catalyst, the supported catalysts is an effective route to improve catalytic activity, and the effect of catalyst support on the catalytic process allow of no neglect. While, the conventional catalyst support such as alumina, silica, carbon materials cannot always fully meet the needs. For example, γ-$A1_2O_3$ with a surface area of 150-300 m^2 g^{-1} is widely used as a catalyst support, but it has poor thermal stability especially under the condition of the feed gas containing water. In additional, γ-$A1_2O_3$ undergoes a phase change to α-$A1_2O_3$ when the temperature is increased to 800 ^oC. The phase transformation significantly results in the decrease of surface area, the closure of pores and the encapsulation of active catalytic sites. Other catalyst support of SiO_2 has the disadvantages of poor alkali resistance, low mechanical strength, easy sintering reunion, and hence cannot meet the demand of the harsh environment.[9, 11, 13-17] Therefore, it is very urgent to find a novel catalyst support to boost catalytic oxidation in rigorous environment. High specific surface area, high thermal conductivity, hydrophobic properties, and good stability are the desired factors to achieve this aim, but how to fabricate such catalyst support is still a great challenge.

Here, we report Ag/white graphene foam for the oxidation of methanol with both high conversion efficiency and high stability. Significantly, the catalyst supports are composed of three-dimensional white graphene foams (the bulk material composed of low-dimensional boron nitride nanosheet, in order to facilitate the writing, called 3D BN) with multi-level pores, atomically thin walls, and specific surface area of 681 m^2 g^{-1}. These structure features endow the white graphene foams superior advantages in the field of catalyst support, and hence the supported Ag catalysts exhibit good catalytic activity and stability. The T_{50} and T_{95} of Ag/white graphene foam catalysts are as low as 50 ^oC and 110 ^oC, almost the half of Ag/γ-Al_2O_3 catalysts. Furthermore, when the temperature was fixed at 100 ^oC, the 93% conversion efficiency of Ag/white graphene foam was well persisted with fluctuation less than 2% within 50 hours, while conversion efficiency of Ag/γ-Al_2O_3 degraded sharply from 46% to 30%.

2 Experiments

2.1 Synthesis methods

In a typical procedure, ammonia borane (AB) was supplied as the B and N source due to its stoichiometric ratio and appropriate decomposition performance, while thiourea as the vesicant in the reaction process for its function in increasing mutual cross-linking between the intermediate products, improving the yield. Thiourea and ammonia borane (AB) with different mass ratio (0:1-5:1) were loaded at the crucible, then placed into the central region of high-temperature tubular furnace, heated to 1100-1400 ^oC under N_2. After the growth of 1-5 h, the furnace was cooled to room temperature and the 3D BN products were synthesized.

The as-grown 3D BN (2 mg mL^{-1}) were dissolved in poly(ethylene glycol) (PEG) by sonication and magnetic stirring. Then the $AgNO_3$ (2 mg mL^{-1}) was added to the solution under the stirring and exposure to a ultraviolet lamp (254 nm) for 30 min. After washing and drying, we can obtain Ag/3D BN samples. The Ag/γ-Al_2O_3 sample (Ag load on the γ-Al_2O_3 support), Ag/C BN sample (Ag load on the commercial BN support) was prepared use the similar method.

2.2 Catalytic performance test

All the catalytic oxidation experiments were performed in a conventional fixed bed continuous-flow reactor under atmospheric pressure. It consists of a stainless steel tube (9 mm i.d.) charged with the required amount of catalyst. An E-type thermocouple was placed in the center of the catalyst bed to control the furnace and record the reaction temperature. The volatile organic compounds (VOCs) laden gas was generated by bubbling air through the VOCs saturators, and then further diluted with another gas steam before reaching the reaction bed. An O_2/N_2 stream through a methanol saturator was mixed with another O_2/N_2 stream. In each test, the molar ratio between O_2 and N_2 is controlled in 5%, 10%, 20%. The concentration of methanol in the feed was regulated in the range of 1000-4000 ppmv by adjusting the saturator temperature, 300 mg of catalyst was placed into the center of the reactor and the total flow rate was kept at 200 mL min^{-1} with a corresponding gas hourly space velocity (GHSV) of 40 000 h^{-1}.

The reaction temperature varied from 20 to 250 ^oC. Prior to the activity studies, the catalyst was activated at 500 ^oC in O_2 for 2 h, and then cooled to room temperature before introducing methanol. All catalytic oxidations were performed in the steady-state condition and started at a temperature that ensured zero conversion of the methanol. The product stream was separated by a capillary column and the VOCs concentrations on the effluent were determined by GC when the composition and concentration of VOCs in the inlet streams were varied, only water and CO_2 were detected in the methanol oxidation. No CO was detected in any experiment. Carbon mass balances were conducted for each set of experimental conditions and the methanol conversion and selectivity to oxidation byproducts were calculated and found to

be within a relative error of less than 5%. The conversions of oxidation were calculated based on the product of CO_2. The reaction was also conducted under various flow rates to test the influence of mass-transfer resistance on the catalyst. No significant rate change was noted, meaning that the mass-transfer limitation was negligible.

2.3 Characterization and application

A field-emission scanning electron microscope (SEM, SU-4800, Hitachi Corp.) and transmission electron microscopy with an energy-dispersive x-ray analyzer (EDX) (TEM or HRTEM, Tecnai F30 S-TWIN, FEI Corp.) were used to investigate the morphology and crystalline structure of the as-prepared 3D BN or Ag/3D BN, respectively. X-ray diffraction (XRD, D8 Advance, Bruker Cu Kα radiation (λ=1.5406 Å)), X-ray photoelectron spectroscopy (XPS, PHI Quantera Ⅱ, and Japan-US Nano Surface Analysis Instruments Corp.) were used to test the composition. Contact angle meter (OCA20, dataphysics) was used to measure the hydrophobic property of 3D BN. Specific surface area test (N_2 adsorption–desorption isotherms, ASAP 2020 M+C, American Micromeritics Corp.) were used to detect the Brunauer Emmett Teller (BET) surface area and non-local density functional theory (NLDFT) pore-size distribution of the as-prepared 3D BN. The N_2 physisorption isotherms were measured at 77 K. Prior to the measurement, the samples were outgassed in vacuum at 300 ^{o}C for 10 h. The BET specific surface area was calculated from the N_2 adsorption data in relative pressure ranging from 0.05 to 0.35. Due to the broad pore size distribution (PSD), ranging from micropores to mesopores, the NLDFT method was used to calculate the pore widths and pore size distributions (ASiQwin software). The ultraviolet spectrophotometer (UV-VIS, UV-3600, Shimadzu Corp.) was used to verify the appearance of silver nanoparticles on the 3D BN. The gas chromatograph (GC, GC7890A, Agilent Corp.) was used to test the catalytic performance of the Ag/3D BN, Ag/γ-Al_2O_3, and pure 3D BN.

3 Result and discussion

Firstly, the white graphene foams were synthesized through thermolysis of thiourea (CN_2H_4S) and ammonia borane (AB) (H_6BN) mixtures. The former acted as vesicants to release a mass of gas during the formation of BN arising from the later raw materials. Fig. 1 presents the fabrication processes of Ag/white graphene foam catalysts. Under ultraviolet (UV) light irradiation, the color variations of pure $AgNO_3$, 3D BN and their mixed solutions were quite different, as show in Fig. 1a. The unchanged 3D BN poly(ethylene glycol) (PEG) solution shows the high stability of 3D BN support under UV radiation. Compared with the slight yellow dyeing of $AgNO_3$ PEG solution, the color of $AgNO_3$/3D BN mixed solution obviously changed from white to dark brown, indicating the 3D BN support shows great influence on the loading process. The colors change is mainly caused by the reducibility of PEG solution and the UV irradiation, through the reduction of Ag ions to atom via electron transfer.[18]

The formation of Ag nanoparticles (Ag NPs) in the mixed solution was further confirmed by the comparison of absorption spectra as shown in Fig. 1b. After irradiation, the local surface plasmon resonance (LSPR) peak of Ag NPs at ~450 nm was very strong from the mixed solution of 3D BN and $AgNO_3$ PEG, very faint from $AgNO_3$ PEG solution, and immeasurable from 3D BN PEG solution.[18, 19]

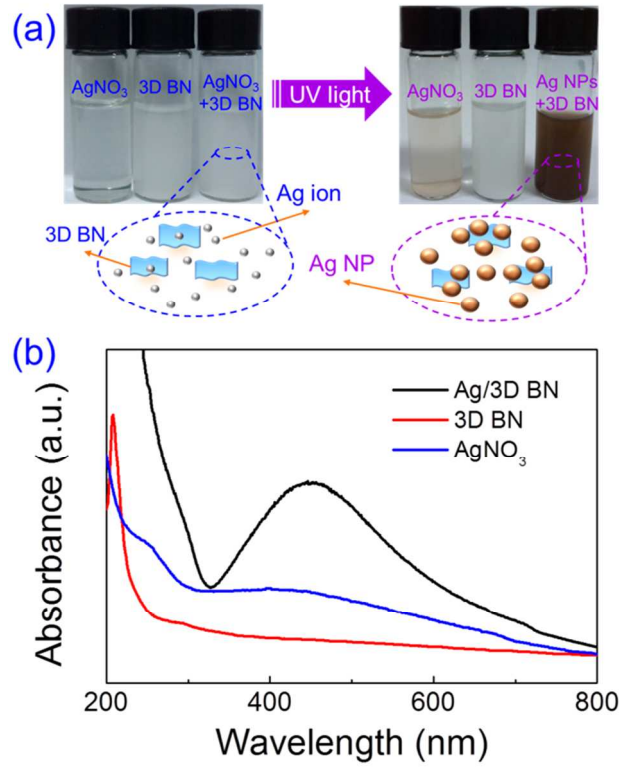

Fig. 1 (a) Photographs of pure $AgNO_3$, 3D BN immersed and their mixed solution before (left) and after (right) ultraviolet irradiation, (b) Comparison of UV–vis absorption spectra of the three kinds of solutions.

The white graphene foams with and without Ag NPs was characterized in Fig. 2. Fig. 2a shows a photo of white graphene foam with length more than 10 cm, demonstrating the large production prepared by the simple thermolysis method which can realize industrial application. During the formation of white graphene foam, the thiourea played an important role,[20, 21] it can promote the mutual crosslinking between the molecules of the transition state of AB, including polymeric aminoborane (PAB), $(H_2BNH_2)_n$, polyiminoborane (PIB), $(HBNH)_n$, borazine ($B_3N_3H_6$), etc.[22, 23] More importantly, thiourea can release a large amount of gas such as, H_2, N_2, NH_3, etc, which initiated and gathered into bubbles and induced volume expansion, significantly improving the production and porosity of boron nitride products. Therefore, we can get the high quality 3D BN with the yield up to 62% compared to the raw materials of AB, far higher than previously reported data (40%).[24] The 3D network-like morphology can be clearly observed from the SEM image as shown in Fig. 2b. This network is composed of irregular skeleton structure and typical flake of the ultra-thin walls with large planar size, as shown in Fig. 2c. Such 3D structure with ultra-thin walls is conducive to improve the loading of silver on the unit mass. In the process of loading silver particles, the structure of 3D BN support exhibits no obvious change even after several hours of ultrasound and magnetic stirring treatment, as shown in Fig. 2d, indicating the structure stability of 3D BN. Fig. 2e reveals the uniform distribution of Ag NPs on the 3D BN

surface.

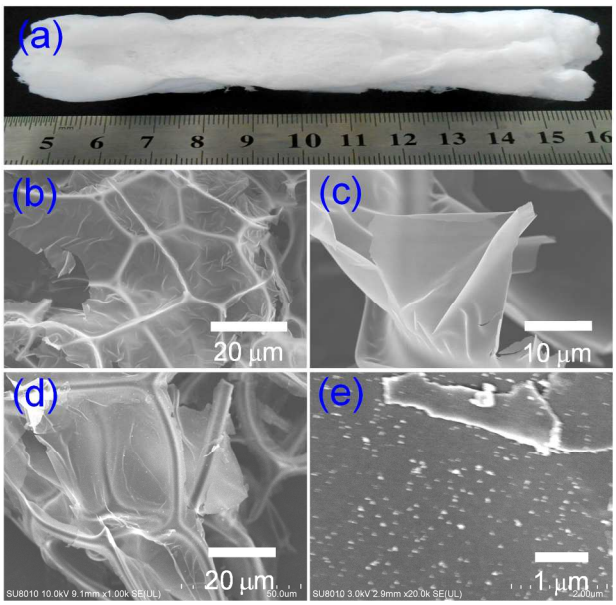

Fig. 2 (a) The photograph of the large production white graphene foam. SEM image of the 3D BN (b, c) and Ag/3D BN (d, e). it is clearly seen that 3D BN is consists of network-like morphology (b) and large lamellar structure with ultra-thin walls (c), the Ag NPs are uniformly distributed on 3D BN (d, e).

The detailed microstructure of Ag/white graphene foam was further characterized by TEM, as shown in Fig. 3. The nanosized pore on BN walls can be clearly found in Fig. 3a. The white graphene foams with large specific surface area (SSA) of 681 m^2 g^{-1} was estimated based on Brunauer-Emmett-Teller (BET) method. The pore volume is 0.58 cm^3 g^{-1}, and the corresponding bipolar pore sizes distribution of 1.5 and 32 nm was observed (supporting information, Fig. S1).[25] Fig. 3b confirms the three layer thickness of lamellar structure, and the layer spacing is about 0.33 nm, which corresponds to the lattice spacing of the h-BN structure (002) plane.[26, 27]

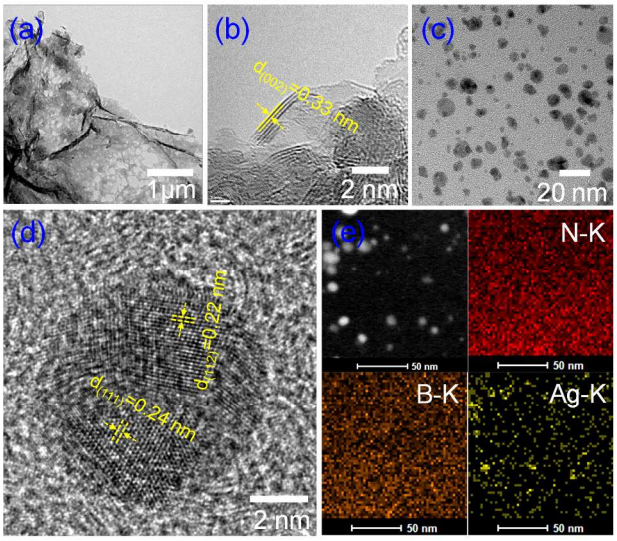

Fig. 3 TEM or HRTEM image of 3D BN (a, b) and Ag/3D BN (c, d). 3D BN exhibits porous microstructure (a) and three layers of lamellar structure (b). TEM images (e) of Ag NPs on 3D BN and corresponding EDX elemental mapping of B, N, Ag.

Fig. 3c reveals that the Ag NPs are uniformly distributed on the BN surface, their average diameter is about 5 nm with size distribution from 2 to 10 nm (Fig. S2). A typical HRTEM of Ag NP is shown in Fig. 3d, Ag (112) and Ag (111) lattice fringes with spacing distances of 0.22 and 0.24 nm are highlighted in yellow line, respectively.[19] Fig. 3e shows the energy dispersive X-ray spectrum (EDX) mapping of B, N, and Ag elements, further confirming the formation of Ag catalysts on the ultrathin BN walls, which is in consistent with the following X-ray photoelectron spectroscopy (XPS) and X-Ray diffraction (XRD) measurements.

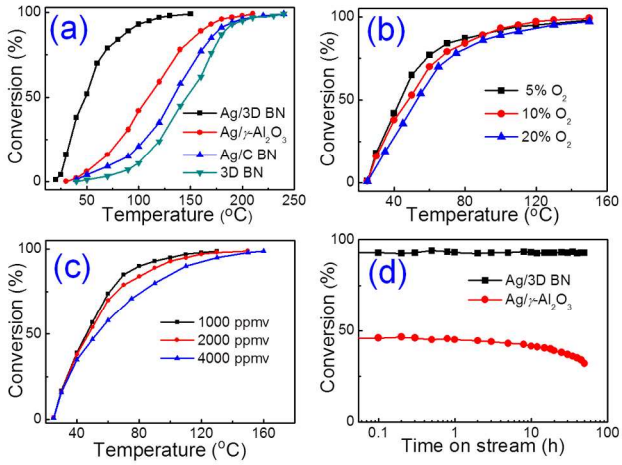

Fig. 4 (a) Temperature-dependent catalytic performance of Ag/3D BN, Ag/γ-Al_2O_3, Ag/C BN (commercial BN), 3D BN, (10% O_2, 2000 ppmv methanol), (b, c) effect of the O_2 (5%, 10%, 20% O_2, 2000 ppmv methanol), methanol (10% O_2, 1000, 2000, 4000 ppmv methanol) concentration on methanol conversion of Ag/3D BN, (d) stability of Ag/3D BN, Ag/γ-Al_2O_3 catalysts for methanol oxidation at 100 °C.

The catalystic performances of Ag/white graphene foam was characterized with oxidation reaction of methanol as shown in Fig. 4. Prior to the reaction activity measurements, the catalysts were activated at 500 °C in O_2 for 2 h.[28, 29] Fig. 4a presents the temperature-dependent conversion efficiencies of methanol to CO_2. Comparing the catalytic activity of pure 3D BN with Ag/3D BN, we can claim that Ag is the primary active site in such oxidation reaction. Comparing the catalytic performance of Ag/C BN (commercial BN) with Ag/3D BN, for the unique structural characteristics of the 3D BN support, make it shows obvious advantages than commercial BN support. The Ag/3D BN exhibit outstanding catalytic activity, which is even much better than conventional Ag/γ-Al_2O_3 catalysts. Generally, the activity of a given catalyst can be mainly characterized by two parameters, T_{50} and T_{95}, corresponding to the temperatures at which the conversion efficiency reaches 50% and 95%, respectively. The activities in catalytic oxidation of several VOCs are summarized in table 1, exhibiting that the Ag/3D BN can be used as an effective catalyst. The light-off temperature (T_{50}) of Ag/3D BN is as low as 50 °C, and the temperature of T_{95} is only 110 °C. For comparison, those two values of Ag/γ-Al_2O_3 are 110 °C and 180 °C, far larger than those of Ag/3D BN. Fig. 4b and 4c show the effects of O_2 and methanol concentrations on catalytic performance of Ag/3D BN. The conversion efficiency slightly

fluctuated with the increase of both O_2 concentration and methanol concentration, which is the typical behavior according to reaction dynamics.[7, 9, 14, 30]

Table. 1 The comparison of different catalysts for VOCs oxidation.

Catalyst	*VOCs*	T_{50} (℃)	T_{95} (℃)	*Reference*
Ag/3D BN	Methanol	50	110	This paper
Ag/γ-Al$_2$O$_3$	Methanol	110	180	This paper
Ag/C BN	Methanol	134	195	This paper
6%Ag/γ-Al$_2$O$_3$	Methanol	135	175	[30]
0.1%Pd/γ-Al$_2$O$_3$	Methanol	187	239	[30]
0.1%Pt/γ-Al$_2$O$_3$	Methanol	169	195	[30]
Pt/h-BN	Iso-hexane	170	300	[11]
Pt/γ-Al$_2$O$_3$	Iso-hexane	260	350	[11]
0.37 wt% Pt/b-BN	Benzene	140	170	[13]
0.37 wt% Pt/a-BN	Benzene	140	175	[13]
Pt/ Al$_2$O$_3$	Benzene	240	280	[13]

Besides activity, stability is also crucial for catalysts. Fig. 4d compares the catalytic stability of Ag/3D BN with Ag/γ-Al_2O_3 when temperature is fixed at 100 °C. The Ag/3D BN catalysts exhibited persistent conversion efficiency around 93% with fluctuation less than 2% within all of the 50 hours measurement. Besides the low conversion efficiency, the degradation of Ag/γ-Al_2O_3 catalysts was so obvious that the conversion rate reduced firstly from 46.5% to 42% in the initial one hour and from 40% to 30% during the period from 10 to 50 hours. The initial degradation of Ag/γ-Al_2O_3 catalysts was induced by the rapid accumulation of water vapor in the micropores due to its high water absorption, and capillary condensation. In a sharp contrast, there was almost no such initial degradation for Ag/3D BN catalysts, which may be attributed to the high hydrophobic feature of white graphene foams with a hydrophobic angle of 131° (Fig. S3). The second degradation of Ag/γ-Al_2O_3 catalysts after long time oxidation reaction is usually attributed to the structural instability and weak thermal conductivity of γ-Al_2O_3.[11, 13, 31] The absence of the long time degradation of Ag/3D BN catalysts is due to the intrinsic properties of BN, such as the high structural stability, high thermal conductivity and hydrophobic property of BN materials. It has been reported that BN can maintain the stability in O_2-containing air at a much higher temperature about 950 °C, and the thermal conductivity can up to 2000 W m^{-1} K^{-1} at room temperature.[26, 27]

The catalytic mechanism of Ag base catalysts has been controversial, but it is generally believed to have a certain relationship with oxygen. The formation of subsurface oxygen (O_γ) was considered necessary for the activation of Ag catalysts for methanol oxidation. Surface-bound atomic oxygen (O_α) preferentially led to the formation of complete oxidation products. The increase of the ratio of O_γ/O_α on the Ag surface would result in an increase in direct methanol oxidation. Recent studies have shown that the Ag-O interaction involving the formation of subsurface oxygen species exerts an important influence on the surface structure and, eventually, the catalytic properties of silver catalysts.[28, 29, 32, 33]

We used X-ray photoelectron spectroscopy (XPS) to detect the chemical states of Ag/3D BN for further understanding of the catalytic mechanism. The survey spectra in Fig. 5a reveals the co-existance of elements B, C, N, O, and Ag. The carbon detected is from surface contamination which is commonly observed by the sensitive XPS method. The detailed B and N peaks are shown in Fig. 5b, in which the main binding energies are located at 190.2 eV and 397.9 eV, respectively. Significantly, compared with symmetric N1s peak, the shape of B1s peak shows obvious asymmetry with a shoulder at 192.1 eV, indicating the appearance of B-O bonds.[34] Meanwhile, the load of Ag and the high temperature O_2 treatment have no much impact on B1s and N1s peaks, the only slight movement of peak position and shape (Fig. S4), indicating that presence interaction between boron nitride and silver, not simple mixed together. Metal-support interactions has an important influence on the catalytic performance. Fig. 5c presents the high resolution of Ag spectra of Ag/3D BN. Obviously, the oxygen activation shifts the Ag $3d_{5/2}$ binding energy from 368 to 367.4 eV, revealing that partial Ag surface has been oxidized into Ag_2O.[29, 35-37] Such speculation about partial surface oxidation was further confirmed by the X-Ray diffraction (XRD) measurements (Fig. S5).

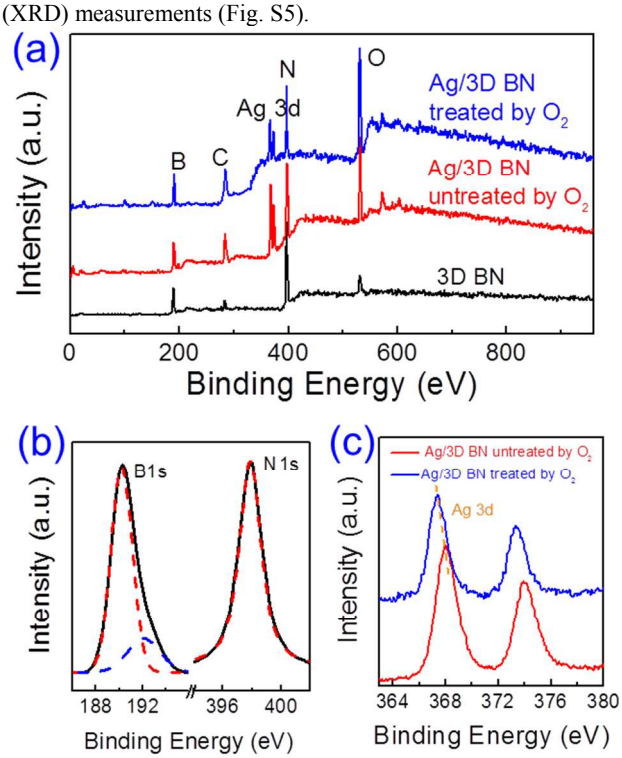

Fig. 5 (a) XPS spectra of the 3D BN, Ag/3D BN before and after O_2 treatment, (b) the detailed B1s, N1s spectra of 3D BN, (c) the detailed Ag 3d spectra of Ag/3D BN before and after O_2 treatment.

The mechanism of 3D BN/Ag catalytic methanol is described in Scheme 1. The high temperature oxygen treatment caused a reconstruction of the Ag surface, forming subsurface oxygen and surface-bound atomic oxygen. The existence of subsurface oxygen facilitates the formation of active sites on silver catalysts, which could enhance the catalytic capability. Surface-bound

atomic oxygen were inclined to form complete oxidation products. 3D BN support provides a moderate surface area that can accommodate dispersed Ag metals, while still preserves the unique characteristics. Furthermore, 3D BN support have the property of high thermal conductivity, temperature stability, acid-base resistance, and hydrophobicity (thus preventing moisture condensation on its surface), which greatly improved the performance of the catalyst. First, methanol and O_2 were adsorbed on the surface of silver then dissociated with improving reactivity, reducing the activation energy and increasing reaction rate. Second, methanol can directly react with oxygen at low temperature to produce H_2O and CO_2. Finally, H_2O and CO_2 molecules desorbed from the surface by diffusion. Then the adsorption-desorption cycle over silver surface was constituted.

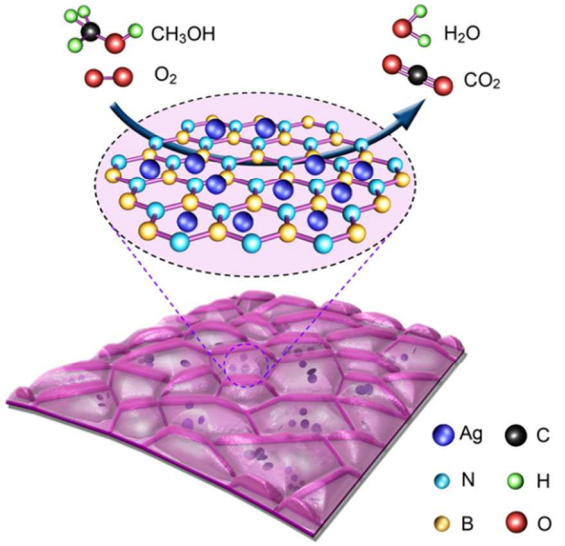

Scheme 1 Illustration the reaction mechanism of Ag/3D BN catalytic methanol.

4 Conclusion

In summary, we apply white graphene foams to replace the usual γ-Al_2O_3 to act as support of Ag catalysts for the high-efficiency catalytic oxidation reaction of methanol. The white graphene foams were fabricated by simple thermolysis method with a large production and can be used as catalyst support to effectively load uniform Ag NPs through UV irradiation. Compared with conventional Ag/γ-Al_2O_3 catalysts, such Ag/3D BN catalysts exhibited much higher catalytic efficiency and better stability. The T_{50} and T_{95} of Ag/3D BN catalysts are as low as 50 ^oC and 110 ^oC, almost the half of Ag/γ-Al_2O_3 catalysts (110 ^oC and 180 ^oC). Within 50 hours of reaction, the 93% conversion efficiency of Ag/3D BN was well persisted with fluctuation less than 2% when the temperature was fixed at 100 ^oC, while the efficiency of Ag/γ-Al_2O_3 degraded sharply from 46% to 30%. Such outstanding catalytic performance of Ag/3D BN catalysts is mainly attributed to the interaction between Ag NP and 3D BN, the unique structure characteristics and the inherent quality of 3D BN. This kind of catalyst shows great potentials in the field of environmental governance and energy applications.

Acknowledgments

This work was supported by the National 973 project from National Basic Research Program of China (2014CB931700), the National Natural Science Foundation of China (61222403), the Doctoral Program Foundation from the Ministry of Education of China (20123218110030), the Fundamental Research Funds for the Central Universities (30920130111017 and NE2012004) and the Opened Fund of the State Key Laboratory on Integrated Optoelectronics (IOSKL2012KF06), Natural Science Foundation for Youths of Jiangsu Province of China (BK20140787), China Postdoctoral Science Foundation funded project (2014M560425) and the Priority Academic Program Development of Jiangsu Higher Education Institutions.

Notes and references

1. Q. Li, Y. Chen, J. R. Rowlett, J. E. McGrath, N. H. Mack and Y. S. Kim, *ACS Appl. Mater. Inter.*, 2014, **6**, 5779-5788.
2. M. Liu, Y. Lu and W. Chen, *Adv. Funct. Mater.* , 2013, **23**, 1289-1296.
3. S. P. Jiang, Z. Liu and Z. Q. Tian, *Adv. Mater.* , 2006, **18**, 1068-1072.
4. Z. Wen, J. Liu and J. Li, *Adv. Mater.* , 2008, **20**, 743-747.
5. T. Yamaguchi, H. Zhou, S. Nakazawa and N. Hara, *Adv. Mater.* , 2007, **19**, 592-596.
6. L. Feng, G. Gao, P. Huang, X. Wang, C. Zhang, J. Zhang, S. Guo and D. Cui, *Nanoscale Res. Lett.* , 2011, **6**, 551.
7. J. H. Lee and D. L. Trimm, *Fuel Process. Technol.* , 1995, **42**, 339-359.
8. M. Zhang, B. Zhou and K. T. Chuang, *Appl. Catal., B-Environ.,* 1997, **13**, 123-130.
9. J. C. S. Wu, Y.-C. Fan and C.-A. Lin, *Ind. Eng. Chem. Res.*, 2003, **42**, 3225-3229.
10. H. Wu, H. Li, Y. Zhai, X. Xu and Y. Jin, *Adv. Mater.*, 2012, **24**, 1594-1597.
11. J. C. S. Wu, Z. A. Lin, J. W. Pan and M. H. Rei, *Appl. Catal. a-Gen.*, 2001, **219**, 117-124.
12. V. M. Ehlinger, K. J. Gabriel, M. M. B. Noureldin and M. M. El-Halwagi, *ACS Sustain. Chem. Eng.*, 2014, **2**, 30-37.
13. C. Lin, *J. Catal.* , 2002, **210**, 39-45.
14. W. R. Schwartz, D. Ciuparu and L. D. Pfefferle, *J. Phys. Chem. C* 2012, **116**, 8587-8593.
15. L. S. Escandon, S. Ordonez, A. Vega and F. V. Diez, *Chemosphere*, 2005, **58**, 9-17.
16. H. Zeng, C. Zhi, Z. Zhang, X. Wei, X. Wang, W. Guo, Y. Bando and D. Golberg, *Nano Lett.* , 2010, **10**, 5049-5055.
17. X. Wang, D.-P. Yang, G. Huang, P. Huang, G. Shen, S. Guo, Y. Mei and D. Cui, *J. Mater. Chem.* , 2012, **22**, 17441-17444.
18. H. Choi, S.-J. Ko, Y. Choi, P. Joo, T. Kim, B. R. Lee, J.-W. Jung, H. J. Choi, M. Cha, J.-R. Jeong, I.-W. Hwang, M. H. Song, B.-S. Kim and J. Y. Kim, *Nat. Photonics* 2013, **7**, 732-738.
19. Y. Lin, C. E. Bunker, K. A. Fernando and J. W. Connell, *ACS Appl. Mater. Interfaces*, 2012, **4**, 1110-1117.
20. X. P. Hao, Y. Z. Wu, J. Zhan, J. X. Yang, X. G. Xu and M. H. Jiang, *J. Phys. Chem. B* 2005, **109**, 19188-19190.
21. X.-L. Meng, N. Lun, Y.-Q. Qi, J.-Q. Bi, Y.-X. Qi, H.-L. Zhu, F.-D. Han, Y.-J. Bai, L.-W. Yin and R.-H. Fan, *Eur. J. Inorg. Chem.* , 2010, **2010**, 3174-3178.

22. G. Wolf, J. Baumann, F. Baitalow and F. P. Hoffmann, *Thermochim. Acta* 2000, **343**, 19-25.
23. D. Neiner, A. Karkamkar, J. C. Linehan, B. Arey, T. Autrey and S. M. Kauzlarich, *J. Phys. Chem. C* 2009, **113**, 1098-1103.
24. X. Wang, A. Pakdel, C. Zhi, K. Watanabe, T. Sekiguchi, D. Golberg and Y. Bando, *J. Phys. Condens. Matter*, 2012, **24**, 314205.
25. K. S. Sing, *Pure Appl. Chem.* , 1985, **57**, 603-619.
26. D. Golberg, Y. Bando, C. C. Tang and C. Y. Zhi, *Adv. Mater.* , 2007, **19**, 2413-2432.
27. X. Song, J. Hu and H. Zeng, *J. Mater. Chem. C*, 2013, **1**, 2952.
28. Z. Qu, M. Cheng, W. Huang and X. Bao, *J. Catal.* , 2005, **229**, 446-458.
29. X. Zhang, Z. Qu, F. Yu and Y. Wang, *J. Catal.* , 2013, **297**, 264-271.
30. W. Wang, H. B. Zhang, G. D. Lin and Z. T. Xiong, *Appl. Catal. B-Environ.*, 2000, **24**, 219-232.
31. J. Mao, M. Deng, L. Chen, Y. Liu and Y. Lu, *AlChE J.* , 2009, **56**, 1545.
32. Z. P. Qu, W. X. Huang, M. J. Cheng and X. H. Bao, *J. Phys. Chem. B* , 2005, **109**, 15842-15848.
33. W.-X. Li, C. Stampfl and M. Scheffler, *Phys. Rev. Lett.* , 2003, **90**, 256102.
34. A. S. Nazarov, V. N. Demin, E. D. Grayfer, A. I. Bulavchenko, A. T. Arymbaeva, H. J. Shin, J. Y. Choi and V. E. Fedorov, *Chem. Asian J.* , 2012, **7**, 554-560.
35. L. Jin, K. Qian, Z. Jiang and W. Huang, *J. Mol. Catal. A: Chem.* , 2007, **274**, 95-100.
36. W. Zhao, L. L. Feng, R. Yang, J. Zheng and X. G. Li, *Appl. Catal. B-Environ.*, 2011, **103**, 181-189.
37. W. W. He, X. C. Wu, J. B. Liu, K. Zhang, W. G. Chu, L. L. Feng, X. A. Hu, W. Y. Zbou and S. S. Me, *J. Phys. Chem. C,* 2009, **113**, 10505-10510.